BIOCHEMICAL AND BIOPHYSICAL RESEARCH COMMUNICATIONS **235,** 47–53 (1997)
ARTICLE NO. RC976732

Single Molecule Imaging of Fluorophores and Enzymatic Reactions Achieved by Objective-Type Total Internal Reflection Fluorescence Microscopy

Makio Tokunaga,* Kazuo Kitamura,*,† Kiwamu Saito,*
Atsuko Hikikoshi Iwane,† and Toshio Yanagida*,†,‡
**Yanagida BioMotron Project, ERATO, JST, Senba-Higashi 2-4-14, Mino, Osaka 562, Japan; †Department of Biophysical Engineering, Osaka University, Toyonaka, Osaka 560, Japan; and ‡Department of Physiology, Osaka University Medical School, Suita, Osaka 565, Japan*

Received April 21, 1997

Imaging of single fluorescent molecules has been achieved in a relatively simple manner using objective-type total internal reflection fluorescence microscopy (TIRFM). Switching from epi-fluorescence microscopy to objective-type TIRFM was achieved by translation of a single mirror in the system. Clear images of single molecules of an orange fluorescent dye, Cy3, were obtained with a fluorescence-to-background ratio of 12, using a conventional high aperture objective (PlanApo, 100 ×, NA 1.4) with ordinary coverslips and immersion oil. This method allowed visualization of single molecules under scanning probe microscopes. Taking advantage of the technique of single molecule imaging, individual ATP turnovers have been visualized with a fluorescent ATP analogue, Cy3-ATP, using a simple experimental strategy. Clear on/off signals were obtained that correspond to the association and dissociation of single Cy3-ATP/ADP molecules with a single myosin head molecule. This method will allow a variety of single-molecular assays of biomolecular functions to be performed using fluorescently labeled substrates, ligands, messengers, and biologically active molecules. Thus, the present technique provides a simple yet powerful and universal tool for researchers to probe the events of single molecules.

Recent years have seen remarkable progress in research on the mechanisms of biological macromolecules at a single-molecular level. In the research field of protein motors, fluorescence microscopy has played a crucial role. Visualization of single actin filaments by fluorescence microscopy (1) lead to the development of new *in vitro* assays for analyzing actomyosin-based molecular motor (2-4) and F1-ATPase rotational motor (5). Forces caused by interactions between motor proteins such as actin-myosin (6-9), kinesin-microtubules (10) and RNA polymerase-DNA (11) have been directly measured using nano-manipulation with microneedles (12) or optical traps (13).

Further advances in technology have made it possible to visualize single fluorescent dye molecules under a fluorescence microscope. As biological molecules function only in aqueous solution, it is critical that they can be visualized in solution. Real time imaging of single fluorophores in aqueous solution has been achieved by refining prism-type total internal reflection fluorescence microscopy (TIRFM) (14) and epi-fluorescence microscopy (14, 15). A major problem to be overcome in visualizing single fluorophores was the huge background light resulting from scattering and luminescence. Illumination by total internal reflection produces an evanescent field just beyond the interface in the medium with a 1/*e* penetration depth of about 150 nm (16), TIRFM has a significant advantage of imaging with a high ratio of fluorescence to background. In the case of prism-type TIRFM, which was used in our previous study, the space just above the coverslip is occupied with a prism, and the working distance of the objective imposes a strict restriction on the thickness of specimens, i.e., they must be thin.

In the present study, imaging of single fluorescent molecules using objective-type TIRFM (prismless TIRFM) (16) has been achieved in a simple yet effective way. In this system, switching from epi-fluorescence microscopy to objective-type TIRFM was achieved by translation of a single mirror in the system. The objective-type TIRFM has the advantage of providing a free space above the coverslip. In addition, there is no limit to the thickness of specimen. These advantages will allow a wide application of the objective-type TIRFM technique, for example, to single-molecular research under scanning probe mi-

0006-291X/97 $25.00

croscopes such as atomic force microscopes (17) and intermolecular force microscopes (18).

In this study, clear on/off signals corresponding to individual ATPase reactions were obtained by objective-type TIRFM using a new fluorescent ATP analogue, 3′(2′)-*O*-Cy3-ATP. In our previous study, individual ATP turnovers were visualized for the first time using another ATP analogue, N^6-Cy3-ATP, by prism-type TIRFM (14). The strategy used was relatively straightforward providing a simple technique, as described here. Therefore, the technique to visualize events of single molecules of enzymatic reactions provide a powerful approach to investigations on the molecular mechanisms of biomolecular functions.

MATERIALS AND METHODS

Proteins. Myosin was extracted from chicken breast (pectoralis) muscle, purified by essentially the method of Szent-Györgyi (19). Myosin subfragment-1 (S1), the head portion of myosin which retains both the actin-binding site and ATPase site, was obtained from chicken myosin by digesting myosin at 20 mg/ml with 10 μg/ml papain (Worthington, USA) in a solution containing 40 mM NaCl, 2 mM $MgCl_2$, 10 mM PIPES, pH 7.0 at 20°C for 15 min (20, 21). Papain was activated by incubating in 5 mM cysteine, 2 mM EDTA, pH 6.2 at 37°C for 30 min just before use. The reaction was stopped by the addition of the cysteine protease inhibitor E64 (Peptide Institute, Japan) to a final concentration of 50 μM. After removal of the insoluble fragments and undigested myosin by centrifugation, proteins precipitated with 67% saturated ammonium sulfate was collected. After dialysis against a purification buffers containing 0.1 M KCl, 10 mM PIPES, pH 7.0, S1 was purified by fast protein liquid chromatography (FPLC) gel filtration chromatography on Superose 6 (Pharmacia, Sweden) with the purification buffer.

A recombinant fusion protein of biotin-dependent transcarboxylase (BDTC) and chicken gizzard smooth muscle regulatory light chain (cgmRLC) was expressed in *E. coli* JM109 (22) and purified according to the method of Trybus and Chatman (23) without using a hydroxylapatite column.

Bovine serum albumin (BSA; fraction V, Sigma, USA) was biotinylated with biotin-$(AC_5)_2$-OSu (Dojindo Laboratories, Japan) in a BSA/biotin molar ratio of 1:20 in 0.1 M $NaHCO_3$, pH 8.5 for 90 min at 25°C, and dialyzed against 25 mM KCl, 10 mM HEPES, 0.02% NaN_3, pH 7.8 (24).

Cy3 labeling of BDTC-cgmRLC. The single cysteinyl residue of BDTC-cgmRLC was labeled with Cy3-maleimide. Cy3-maleimide was prepared by coupling Cy3-OSu (Cy3.29.OSu, 100 nmole; Biological Detection Systems, USA) (25) with *N*-[2-(1-piperazinyl)ethyl]-maleimide (90 nmole, Dojindo Laboratories, Japan) in 25 μl DMSO at 40°C overnight. Just prior to use, glycine was added (5 mM, final concentration in reaction mixtures with protein to be labeled) to block the unreacted *N*-hydroxysuccinimide ester. BDTC-cgmRLC in a solution containing 0.6 M NaCl, 2 M guanidine-HCl, 10 mM HEPES pH 7.0 was mixed with Cy3-maleimide in a cgmRLC/Cy3 molar ratio of 1:5. After incubation for 2 hours at 25°C, unreacted dyes were removed with a Sephadex G-25 column (NAP-5, Pharmacia, Sweden) in 0.5 M NaCl, 50 mM PIPES, 10 mM EDTA, 10 mM DTT, pH 7.0.

Preparation of Cy3-BDTC-S1. The endogenous RLC of S1 was exchanged for Cy3-BDTC-cgmRLC according to the method reported previously (23, 26, 27) with some modifications. Papain-digested S1 was incubated with a 10-fold molar excess of Cy3-BDTC-S1 in an exchange buffer (0.5 M NaCl, 50 mM PIPES, 10 mM EDTA, 10 mM DTT, 10 mM ATP, pH 7.0) for 20 min at 40°C. The reaction was terminated by the addition of $MgCl_2$ to a final concentration of 12 mM and cooled on ice. The hybrid myosin S1 (Cy3-BDTC-S1) was subsequently separated from the excess Cy3-BDTC-cgmRLC and the displaced RLC by FPLC gel filtration chromatography on Superose 6 (Pharmacia, Sweden) with buffers containing 0.1 M KCl, 10 mM PIPES, 1 mM $MgCl_2$, pH 7.0. The degree of Cy3 labeling of Cy3-BDTC-S1 was estimated to be approximately 100% using molar absorption coefficients of 150,000 $M^{-1}cm^{-1}$ at 552 nm, 12,000 $M^{-1}cm^{-1}$ at 280 nm for Cy3 and absorption coefficients of 0.83 $(mg/ml)^{-1}cm^{-1}$ and 0.2 $(mg/ml)^{-1}cm^{-1}$ at 280 nm for S1 and BDTC-RLC, respectively. Molecular weights of 32,000, 132,000 and 145,000 were used for BDTC-cgmRLC, S1 and BDTC-cgmRLC-S1, respectively.

Cy3-ATP. 3′(2′)-*O*-[*N*-[2-[(Cy3)amino]ethyl]carbamoyl]-ATP (Cy3-ATP) was prepared by coupling 3′(2′)-*O*-[*N*-[2-(amino)ethyl]-carbamoyl]-ATP (29 μM) (28, 29) with the *N*-hydroxysuccinimide ester of Cy3.29 (Cy3-OSu, 900 nmole; Biological Detection Systems) (25) in 400 ml of 0.5 M triethanolamine, pH 8.5 at 25°C for 3 hours. After pH was neutralized, unreacted aminoethylcarbamoyl-ATP and Cy3 was removed by FPLC reverse phase chromatography on Resource RPC (Pharmacia). The Cy3-ATP fraction was further purified by FPLC anion-exchange chromatography on Mono Q (Pharmacia). The pooled fractions were freeze dried. The final product was dissolved in water and stored at −80°C.

Microscopy. A high numerical aperture objective (OL) (PlanApo, 100×, NA = 1.4, infinity corrected; Olympus, Japan) was mounted on a nose piece of an inverted microscope (Infinity optical system; IX70, Olympus) (Fig. 1). The microscope system was set up in a clean room to reduce the chance of dust particles. A laser beam from a diode pumped Nd:YAG laser (wave length = 532 nm, 20 mW, linearly polarized; μ green laser, model 4301-020, Uniphase, USA) was attenuated by neutral density filters (ND) and expanded by a lens (L1, f = 15 mm). After conversion into circular polarization by a quarter-wave plate ($\lambda/4$), the laser beam was focused by a lens (L2, f = 350 mm) on the back focal plane of the objective so that specimens were illuminated by paraxial rays with Koehler illumination. The power of the incident laser was 1.7 mW at the nose piece. Since the numerical aperture of the beam was adjusted to 0.025 with a diaphragm (A), the laser beam illuminated an area of approximately 40 μm × 50 μm at the specimen plane. The laser beam was reflected by a mirror (M) before being reflected by a dichroic mirror (DM) (DM532, Asahi Spectrum, Japan). Illumination was switched between epi-fluorescence microscopy and objective-type TIRFM by simply shifting the position of the mirror (M).

The background of scattered light was rejected with a holographic notch filter (NF) (HNPF-532AR-1.0, Kaiser Optical System, USA), whose optical density at 532 nm was larger than 6, and an interference band pass filter 590DF60 (transmission wavelength = 560-620 nm; Omega Optical, USA). Imaging and photon counting were performed simultaneously, by splitting the beam with a half mirror (HM). An intermediate image (I2) formed by spherical achromatic lenses (L3, L5, f = 100 mm) was enlarged by a projection lens (PL) (PE5×, Olympus).

Non-fluorescent immersion oil (for ordinary use, nd=1.516, Olympus, Japan) is suitable for single molecule fluorescence imaging because it emits low fluorescence and has adequate viscosity. Glass coverslips (thickness No. 1, 24×32mm, Matsunami, Japan) were cleaned with 0.1 M KOH and washed thoroughly with water before use and stored in water. Flow cells were freshly constructed from a cleaned coverslip and a smaller coverslip, separated by thin strips of polymer sheet (approximately 50 μm thick). Milli-Q (Millipore, USA) water was used in all the experiments.

Images were recorded with an ISIT camera, composed of an image intensifier (VS4-1845, Video Scope International, USA) and a SIT camera (C2400-08, Hamamatsu Photonics, Japan), and stored on S-VHS videotape. Video-taped images were processed with a digital image processor (Argus-20, Hamamatsu Photonics).

Photon counting. The intermediate image I1 was magnified 3 diameters by spherical achromatic lenses L3 and L4 (L3, f = 100 mm;

L4, f = 300 mm). Thus, a 300 × magnified image was formed on an avalanche photodiode of a single photon counting module (SPCM-200-PQ CD1705, EG&G Optoelectronics, Canada). Since the diameter of the efficient detection area of the avalanche photodiode was approximately 150 μm, photons emitted from an area 0.5 μm in diameter at the specimen plane were counted. Its dimensions (0.5 μm in diameter) were decided to be almost the same as that of the Airy disk. Signal pulses from the photon counting module were counted with a gate time of 100 msec using a photon counting board (M3949, Hamamatsu Photonics) that resided in a personal computer (PC9801FA, NEC, Japan). The specimen stage (Σ-262CH-S, Sigma Koki) was equipped with DC-motor positioners (DMY-25, Sigma Koki, Japan) and piezoelectric actuators (DPT-C-S, Queensgate Instruments, England), which were controlled by computer. By scanning with a computer program, the fluorescent spot was positioned at the correct location so that its image was formed exactly at the center of the avalanche photodiode.

Single molecule imaging of Cy3-S1. A small aliquot of 35 pM Cy3-BDTC-S1 in a assay buffer (25 mM KCl, 5 mM $MgCl_2$, 20 mM PIPES, pH 7.8) was introduced into the flow cell. After washing with the assay buffer, the bathing solution was replaced by the assay buffer containing an oxygen reduction system (4.5 mg/ml glucose, 36 μg/ml catalase, 216 μg/ml glucose oxidase and 1% (v/v) 2-mercaptoethanol) (12, 30).

ATPase reactions. The surface of a cleaned coverslip was coated with biotinylated BSA by introducing 1 mg/ml biotinylated BSA in the assay buffer into the flow cell. After rinsing with the assay buffer, 1 mg/ml streptavidin (Molecular Probes, USA) in the assay buffer was introduced and allowed to bind to the immobilized biotin for 10 min. After rinsing, 35 pM Cy3-BDTC-S1 in the assay buffer was then introduced and allowed to bind to the immobilized streptavidin for 5 min. After washing out unbound Cy3-BDTC-S1 with the assay buffer, the bathing solution was replaced with the assay buffer containing 50 nM Cy3-ATP and an oxygen reduction system. All procedures for specimen preparation were carried out in the clean room to avoid dust contamination. After the flow cell was sealed with nail varnish, the specimen was examined by microscopy at 25 °C. To exclude the influence of photobleaching, the power of the incident laser was decreased to 0.8 mW at the nose piece so that the fluorescence lifetime of Cy3 became long (about 2 min).

RESULTS AND DISCUSSION

Objective-Type Total Internal Reflection Fluorescence Microscopy

To visualize single fluorescent dye molecules, objective-type TIRFM (prismless TIRFM) (16) was applied (Fig. 1) instead of prism-type TIRFM, which was used in our previous study (14). A method to switch simply between epi-fluorescence microscopy and objective-type TIRFM was developed. Changing the position of the mirror (M) shifted the incident beam path from the center to the edge of the objective lens as illustrated in Fig. 1. Thus, the change of illumination was achieved only by shifting a single mirror. This new method simplified both the optical system and the experimental procedure.

Imaging of Single Cy3 Molecules by Objective-Type TIRFM

Clear images of single fluorescent dye molecules were obtained by objective-type TIRFM (Fig. 2A) using a conventional high aperture objective (PlanApo, 100 ×, NA 1.4) with ordinary glass coverslips and immersion oil. An orange fluorescent dye, Cy3 (absorbance maximum 552 nm, emission maximum 565 nm) (25) was covalently bound to the single cysteinyl residue of a recombinant fusion protein, BDTC-cgmRLC. The endogenous RLC of S1 was then exchanged for Cy3-BDTC-cgmRLC. The resulting single Cy3-BDTC-S1 molecules contained single Cy3 molecules. Cy3-BDTC-S1 molecules were examined using objective-type TIRFM. As shown in figure 2A, single Cy3-BDTC-S1 molecules produced clear fluorescent spots.

Evidence that single fluorescent spots were produced from single Cy3 molecules by objective-type TIRFM was obtained as follows: 1) The fluorescent spots were bleached in a single step (Fig. 2B). 2) The intensity

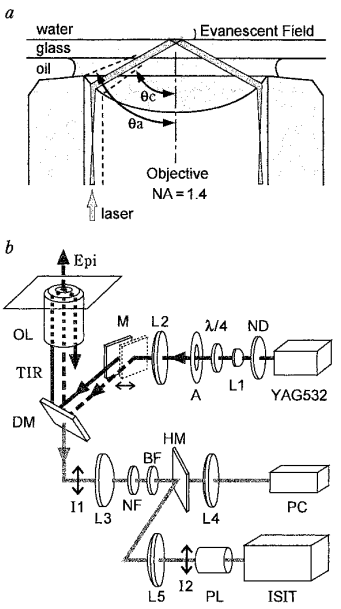

FIG. 1. (a) Schematic drawing of objective-type TIRFM (prismless TIRFM) (16). The incident laser beam was focused on the back focal plane of the objective lens with a numerical aperture (NA) of 1.4. θa (67.1°) is the angle corresponding to NA (1.52 $\sin\theta a$ = NA; 1.52 is the reflective index of glass). θc (61.0°) is the critical angle of the glass-water interface (1.33 $\sin 90° = 1.52 \sin\theta c$; 1.33 is the reflective index of water). When the incident beam was positioned to propagate along the objective edge between θa and θc, the beam was totally internally reflected producing an evanescent field at the glass-water interface (1/*e* penetration depth is about 150 nm). (b) Schematic drawing of the microscope used for single molecule imaging of fluorescent molecules employing objective-type TIRFM. Switching between epi-fluorescence microscopy and objective-type TIRFM was performed by a simple method, i.e., by translating a single mirror (M). YAG532, diode pumped Nd:YAG laser (532 nm); ND, neutral density filters; L1, lens for beam expansion; λ/4, quarter-wave plate; A, diaphragm; L2, focusing lens; M, mirror to change the laser path; DM, dichroic mirror to introduce the laser into the objective lens; OL, objective lens; I1, I2, intermediate image; L3, L4, L5, spherical achromatic lens for image formation; NF, notch filter to block incident light (532 nm); BF, bandpass filter; PC, single photon counting module; PL, projection lens; ISIT, image-intensified SIT camera.

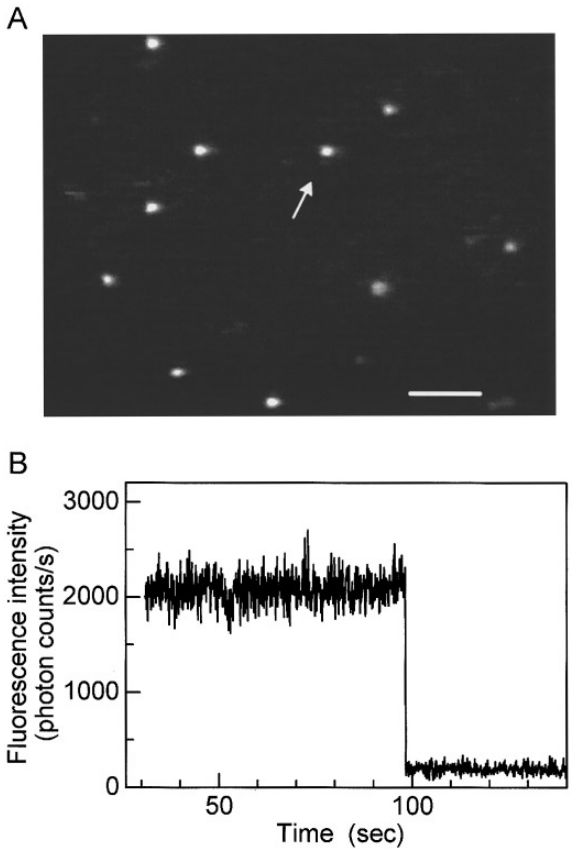

FIG. 2. (A) Fluorescence images of single, Cy3-labeled myosin head (Cy3-S1) molecules by objective-type TIRFM. The images were recorded at the video rate (1/30 s) with an ISIT camera. The micrograph shown is the average over 16 frames. The power of the incident laser was 1.7 mW at the nose piece, and an area of approximately 40×50 μm at the specimen plane was illuminated. Scale bar, 5 μm. (B) Quantized photobleaching of a fluorescent molecule indicated by the arrow in (A), proving that the single fluorescent spot was produced from a single Cy3 molecule.

distribution of fluorescent spots exhibited a single peak (Fig. 3A). 3) The lifetime distribution of fluorescence displayed a single exponential curve (Fig. 3B), suggesting that the bleaching event followed a single Poisson process.

Fluorescence-to-Background Ratio of Single Molecule Imaging

Reduction of the background intensity of fluorescence images, which is mainly caused by scattered light including Raman scattering, is the key point in achieving single molecule imaging (14). Improving the microscope optical system using a laser beam has significantly reduced the background light compared with conventional epi-fluorescence microscopy using a mercury lamp. Although a ordinary objective, coverslip and immersion oil have been used, the background intensity of both objective-type TIR illumination and the improved epi-illumination was remarkably low (Table 1, Cy3-S1). This low background has made it possible to visualize single Cy3 molecules by using this improved epi-fluorescence microscopy with a fluorescence-to-background ratio of 2.9 (Table 1, Cy3-S1).

The reasons why the background light has been significantly reduced compared with conventional epi-fluorescence is as follows: a laser beam has been used, only a small area has been illuminated, scattered light has been rejected by both the filters (notch filter and band-pass filter) and the dichroic mirror. In the previous study, very low background intensity was achieved by prism-type TIRFM using a fluorescence-less objective, quartz coverslips and slides, non-fluorescent special immersion oil, and optical parts made of fused silica (14). This is approximately 50 times lower than that produced by objective-type TIRFM when a conventional objective, coverslip, immersion oil and glass optical parts were used. However, the latter is practically low enough to produce clear images of single Cy3 molecules using objective-type TIRFM, as shown in Fig. 2A.

High-contrast fluorescence images of single Cy3 molecules by objective-type TIRFM were achieved not only by significantly reducing the background light but also by increasing the fluorescence intensity produced by single Cy3 molecules. Switching from epi-illumination to objective-type TIR illumination increased the fluorescence intensity from single Cy3 molecules 3-fold (Table 1, Cy3-S1), although the light intensity incident to the objective was the same. The increase in the single

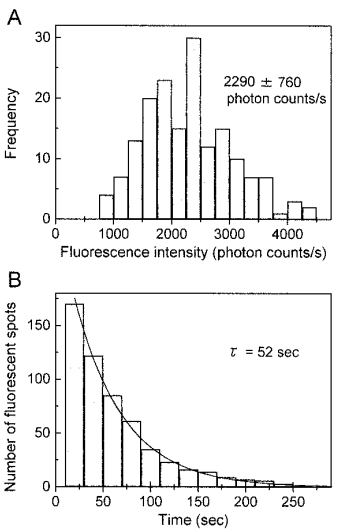

FIG. 3. (A) Distribution of fluorescence intensities from Cy3-S1. The intensity of each fluorescent spot was counted with the single photon counting module. The distribution shows a single peak providing evidence that the spots are the image of single molecules. (B) Distribution of the fluorescence lifetimes of Cy3-S1. The number of spots that remained fluorescent after the start of illumination has been plotted. The distribution displayed a single exponential curve, suggesting that the bleaching event followed a single Poisson process.

TABLE 1

Fluorescence Intensity Emitted from Single Cy3 Molecules

Sample	Illumination	Fluorescence[a] (photon counts/s)	Background (photon counts/s)	Fluorescence/ background[b]
Cy3-S1	TIR[c]	2290 ± 760 (169)	190 ± 20 (169)	12
	Improved epi[d]	730 ± 360 (36)	250 ± 20 (36)	2.9
Cy3-ATP (50 nM)	TIR[c]	2650 ± 650 (81)	4180 ± 600 (81)[f]	0.63
	Improved epi[d]	ND[e]	24200 ± 6900 (27)[f]	~0.03[g]

Note. Values are means ± standard deviation (*n*). The intensity of fluorescence and background was measured using a single photon counting module. The power of the incident laser was 1.7 mW at the nose piece, and an area of approximately 40 × 50 μm at the specimen plane was illuminated.

[a] Fluorescence intensity emitted from single Cy3 molecules.

[b] Ratio of the single molecule fluorescence intensity to the background intensity.

[c] Illumination by objective-type total internal reflection (TIR).

[d] Improved epi-illumination using a laser beam. The light intensity incident to the objective was the same as that of TIR illumination. Note that the conventional epi-illumination using a mercury lamp gives significantly higher background light.

[e] ND, not detected.

[f] Higher background resulting from free Cy3-ATP in solution.

[g] This value was obtained by assuming that the fluorescence intensity is the same as that emitted from Cy3-S1.

molecule fluorescence is due to a greater evanescent field intensity produced by TIR than the incident light intensity (16). As a result, clear fluorescent spots of single Cy3 molecules were obtained with a fluorescence-to-background ratio of 12.

Single Molecule Imaging of Individual ATP Turnovers

Events of single molecules of ATPase reactions have been visualized with a new fluorescent ATP analogue, 3′(2′)-*O*-Cy3-ATP (Fig. 4a). As reported in our previous paper, individual ATP turnovers were visualized for the first time using another ATP analogue, N^6-Cy3-ATP, by prism-type TIRFM (14). Initially we intended to visualize phosphate ion, the product of ATPase reaction, on the analogy of fluorescent calcium indicators. This probed to be very difficult. Instead, a relatively simple strategy was adopted (Fig. 4b) and is described as follows: 1) Individual ATP turnovers can be visualized using fluorescence emitted from single Cy3-ATP molecules with the aid of Brownian motion, instead of changes in fluorescence brought about by enzyme-ATP interactions. When Cy3-ATP or Cy3-ADP is associated with the enzyme, it can be visualized as a clear fluorescent spot, whereas free Cy3-ATP or Cy3-ADP undergoing rapid Brownian motion is not seen as a discrete spot. 2) The background fluorescence produced by free Cy3-ATP can be remarkably reduced by TIRFM, because the illuminated region is localized very close to the glass-water interface (1/*e* penetration depth is about 150 nm). 3) If 10 nM Cy3-ATP is applied, on average there will be one Cy3-ATP molecule in a volume of 1 μm square area × 200 nm depth. Therefore, the background fluorescence is low enough to visualize single Cy3 molecules. The concentration of 10 nM appears to be too low; however, the ATPase reaction occurs because the concentration of 10 nM is much higher than the association constant of ATP to myosin, which is in the picomolar concentration range.

The fluorescence intensity from Cy3-ATP corresponded with that of Cy3-S1 within error as shown in Table 1. Free Cy3-ATP in solution caused higher background fluorescence. When the Cy3-ATP concentration was increased to 50 nM, the background fluorescence by epi-illumination was too high to detect single Cy3 molecules. In the case of objective-type TIRFM, the fluorescence-to-background ratio was 0.6 at 50 nM Cy3-ATP. Therefore, single molecule imaging of ATPase reactions could be achieved at this concentration.

Clear on/off signals were obtained which corresponded to the association and dissociation of single Cy3-ATP/ADP molecules with a single S1 molecule (Fig. 4c). Cy3-BDTC-S1, whose BDTC was a biotinylated peptide and located at the distal end of S1, was attached to the glass surface by the tail end of S1 in a specific manner using a biotin-avidin system. A fluorescent spot of a single Cy3-BDTC-S1 molecule was positioned at the correct location which corresponded to the center of the detector of the single photon counting module. After photobleaching of the Cy3 dye of Cy3-BDTC-S1, individual ATP turnovers by the single S1 molecule was detected by directly measuring association-(hydrolysis)-dissociation of Cy3-ATP with the single photon counting module.

The lifetime of bound Cy3-ATP or Cy3-ADP followed a exponential decay function with a lifetime of 9 sec at 25°C (data not shown), which is consistent with the Mg-ATPase activity of BDTC-S1 suspended in solution (0.09 Pi/sec/head at 25°C). This result indicates that

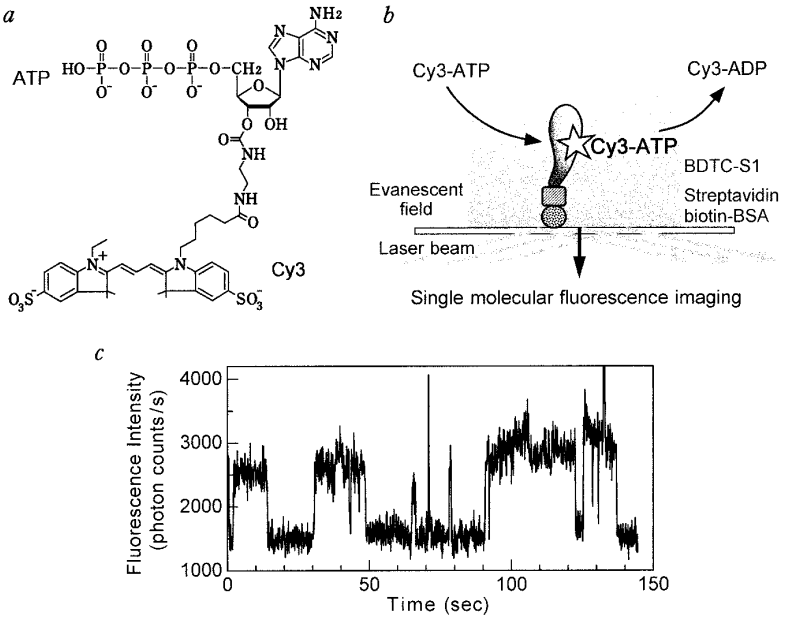

FIG. 4. Single molecule imaging of individual ATP turnovers by single S1 molecules. (a) Structure of 3′(2′)-*O*-[*N*-[2-[(Cy3)amino]ethyl]-carbamoyl]-ATP (Cy3-ATP). (b) Schematic diagram illustrating how the ATPase reaction could be visualized with Cy3-ATP using objective-type TIRFM (see text). (c) Photon-counted fluorescence intensity of a single Cy3-ATP (or hydrolyzed Cy3-ADP) on a single BDTC-S1 molecule. On/off signals correspond to the association and dissociation of single Cy3-ATP/ADP molecules with a single myosin head molecule. To exclude the influence of photobleaching, the power of the incident laser was decreased to 0.8 mW at the nose piece so that the fluorescence lifetime of Cy3 became long (about 2 min). Note that the lower laser power resulted in lower counts of the fluorescence and background intensity.

BDTC-S1 molecules retain their ATPase activity even when bound to a glass surface at very low density (less than one molecule per 1 μm square). This corresponds well to the finding that BDTC-S1 retained its sliding activity when it was bound to the surface at normal density by its tail end using the same method (22). In this study the ribose-modified fluorescent ATP analogue 3′(2′)-*O*-Cy3-ATP was used, and both the Mg^{2+}-ATPase activity and actin-activated ATPase activity of 3′(2′)-*O*-Cy3-ATP by S1 in solution was similar to that of unlabeled ATP. Thus, all the present methods involving protein incorporation onto glass surfaces and fluorescence labeling of the proteins and ATP do not damage the activity of the molecules. This results in clear visualization of single ATPase reactions which are consistent with the results obtained in solution using unlabeled proteins and ATP.

Advantages of the Newly Developed Microscopy

In the present study, imaging of single fluorescent molecules using objective-type TIRFM has been achieved in a relatively simple manner using a conventional high aperture objective with ordinary coverslips and immersion oil. A new method for switching between epi-fluorescence microscopy and objective-type TIRFM simplified both the optical system and the experimental procedure. The background intensity by objective-type TIRFM using conventional optical parts is practically low enough to obtain clear images of single Cy3 molecules with a fluorescence-to-background ratio of 12. Objective-type TIRFM has no limit to the thickness of specimen, whereas prism-type TIRFM has a strict restriction imposed on the thickness of specimens. The present microscopy enables, for example, single-molecular examination of the surfaces of thick cells or tissues and the surfaces of specimens with low transmittance.

Furthermore, a free space is provided above the specimen, which is occupied by a prism in the case of prism-type TIRFM. Taking advantage of this free space, single molecule imaging can be achieved under manipulating systems and scanning probe microscopes such as atomic force microscopes (17) and intermolecular force microscopes (18). Indeed, direct trapping of single protein molecules onto the tip of probes has been achieved while monitoring single molecules by objective-type TIRFM (31).

Single molecule imaging of ATPase reactions has been achieved, and clear on/off signals corresponding to the association and dissociation of single fluorescent ATP/ADP molecules have been obtained using a new fluorescent ATP analogue, 3′(2′)-*O*-Cy3-ATP. The strategy is relatively simple. In addition, many substrates, ligands, messengers and biologically active molecules can be labeled fluorescently. Only a very few molecules (attomole to femtomole range) are required

for detection, because single-molecular assays are carried out in the picomolar to nanomolar concentration range. Thus, the technique of single-molecular assays described here provides a powerful and universal tool for single-molecular investigations on many kinds of biomolecular functions leading to a wide spread use of its application.

ACKNOWLEDGMENTS

We are grateful to the members of the ERATO project for valuable discussions and to Dr. Jan West for critical reading of the manuscript and valuable comments.

REFERENCES

1. Yanagida, T., Nakase, M., Nishiyama, K., and Oosawa, F. (1984) *Nature (London)* **307,** 58–60.
2. Kron, S. J., and Spudich, J. A. (1986) *Proc. Natl. Acad. Sci. USA* **83,** 6272–6276.
3. Harada, Y., Noguchi, A., Kishino, A., and Yanagida, T. (1987) *Nature (London)* **326,** 805–808.
4. Saito, K., Aoki, T., Aoki, T., and Yanagida, T. (1994) *Biophys. J.* **66,** 769–777.
5. Noji, H., Yasuda, R., Yoshida, M., and Kinosita Jr, K. (1997) *Nature (London)* **386,** 299–302.
6. Ishijima, A., Doi, T., Sakurada, K., and Yanagida, T. (1991) *Nature (London)* **352,** 301–306.
7. Finer, J. T., Simmons, R. M., and Spudich, J. A. (1994) *Nature (London)* **368,** 113–119.
8. Molloy, J. E., Burns, J. E., Kendrick-Jones, J., Tregear, R. T., and White, D. C. S. (1995) *Nature (London)* **378,** 209–212.
9. Ishijima, A., Kojima, H., Higuchi, H., Harada, Y., Funatsu, T., and Yanagida, T. (1996) *Biophys. J.* **70,** 383–400.
10. Svoboda, K., Schmidt, C. F., Schnapp, B. J., and Block, S. M. (1993) *Nature (London)* **365,** 721–727.
11. Yin, H., Wang, M. D., Svoboda, K., Landick, R., Block, S. M., and Gelles, J. (1995) *Science* **270,** 1653–1657.
12. Kishino, A., and Yanagida, T. (1988) *Nature (London)* **334,** 74–76.
13. Ashkin, A., Dziedzic, J. M., Bjorkholm, J. E., and Chu, S. (1986) *Opt. Lett.* **11,** 288–290.
14. Funatsu, T., Harada, Y., Tokunaga, M., Saito, K., and Yanagida, T. (1995) *Nature (London)* **374,** 555–559.
15. Sase, I., Miyata, H., Corrie, J. E. T., Craik, J. S., and Kinosita Jr, K. (1995) *Biophys. J.* **69,** 323–328.
16. Axelrod, D. (1989) *Meth. Cell Biol.* **30,** 245–270.
17. Binnig, G., Quate, C. F., and Gerber, C. (1986) *Phys. Rev. Lett.* **56,** 930–933.
18. Tokunaga, M., Aoki, T., Hiroshima, M., Kitamura, K., and Yanagida, T. (1997) *Biochem. Biophys. Res. Commun.* **231,** 566–569.
19. Szent-Györgyi, A. (1951) Chemistry of Muscular Contraction, 2nd ed., Academic Press, New York.
20. Margossian, S. S., Stafford, W. F. 3rd, and Lowey, S. (1981) *Biochemistry* **20,** 2151–2155.
21. Wakabayashi, K., Tokunaga, M., Kohno, I., Sugimoto, Y., Hamanaka, T., Takezawa, Y., Wakabayashi, T., and Amemiya, Y. (1992) *Science* **258,** 443–447.
22. Iwane, A. H., Kitamura, K., Tokunaga, M., and Yanagida, T. (1997) *Biochem. Biophys. Res. Commun.* **230,** 76–80.
23. Trybus, K. M., and Chatman, T. A. (1993) *J. Biol. Chem.* **268,** 4412–4419.
24. Itakura, S., Yamakawa, H., Toyoshima, Y. Y., Ishijima, A., Kojima, H., Harada, Y., Yanagida, T., Wakabayashi, T., and Sutoh, K. (1993) *Biochem. Biophys. Res. Commun.* **196,** 1504–1510.
25. Mujumdar, R. B., Ernst, L. A., Mujumdar, S. R., Lewis, C. J., and Waggoner, A. S. (1993) *Bioconjugate Chemistry* **4,** 105–111.
26. Katoh, T., and Lowey, S. (1989) *J. Cell Biol.* **109,** 1549–1560.
27. Rajasekharan, K. N., Morita, J., Mayadevi, M., Ikebe, M., and Burke, M. (1991) *Arch. Biochem. Biophys.* **288,** 584–590.
28. Cremo, C. R., Neuron, J. M., and Yount, R. G. (1990) *Biochemistry* **29,** 3309–3319.
29. Sowerby, A. J., Seehra, C. K., Lee, M., and Bagshaw, C. R. (1993) *J. Mol. Biol.* **234,** 114–123.
30. Harada, Y., Sakurada, K., Aoki, T., Thomas, D. D., and Yanagida, T. (1990) *J. Mol. Biol.* **216,** 49–68.
31. Kitamura, K., Tokunaga, M., Iwane, A. H., Saito, K., and Yanagida, T. (1997) *Biophys. J.* **72,** A55.